nature geoscience

SUPPLEMENTARY INFORMATION

DOI: 10.1038/NGEO433

Supporting Information for

Preservation of Iron(II) by Carbon-Rich Matrices in a Hydrothermal Plume

Brandy M. Toner*, Sirine C. Fakra, Steven J. Manganini, Cara M. Santelli, Matthew A. Marcus, James W. Moffett, Olivier Rouxel, Christopher R. German, and Katrina J. Edwards

*To whom correspondences should be addressed. Email: toner@umn.edu.

This file contains:

Text (1810 words)
Figure captions (477 words)
Fig.S1 – Fig.S6
4 References

Synopsis of Nano-probe Spectroscopic Measurements – Below is a synopsis of our nano-probe spectroscopic measurements, what they tell us about our hydrothermal plume samples, and how they bring us to the conclusion that Fe(II) is complexed by the POC:

- ***Scanning Transmission X-ray Microscopy (STXM)***
  STXM is a transmission microscopy technique that relies on the photon absorption contrast mechanism (30nm spatial resolution). Fig.1a area 3 demonstrates the appearance of mineral particles as clusters of nanoparticulate ferrihydrite. When we observe areas of the sample with *evenly dispersed* Fe, like Fig.1a area 2, we may conclude that the Fe is dissolved, sorbed, or in a uniformly distributed particulate form with a particle size << 30 nm. We can dismiss the dissolved Fe explanation – these samples were rinsed with purified water prior to analysis. Any remaining dissolved Fe should be well below our detection limit of ~0.1 mM for dissolved species [1]. We dismiss an Fe-bearing mineral particle form based on spectroscopic evidence discussed below (Fe L-edge NEXAFS). The remaining explanations are: (1) Fe is sorbed or complexed in a fairly uniform

DOI: 10.1038/NGEO433

manner to the background matrix or (2) Fe is in a non-mineral particle form distributed uniformly thorough out the background matrix. From the C maps, we know that the background matrix is rich in C.

- ***Near Edge X-ray Absorption Fine Structure (NEXAFS) Spectroscopy***

Fe L-edge NEXAFS spectra are sensitive to both Fe oxidation state and Fe local bonding environment. The relative concentration of each Fe form (II and III) is reflected in the amplitude of the two peaks at 707.6 and 709.5 eV, respectively. The Fe NEXAFS spectra tell us clearly that there are particle aggregates dominated by Fe(III) – these are ferrihydrite-like minerals (e.g. Fig.1b and Fig.S5). The Fe spectra also tell us that there is Fe(II) in the background C-rich matrix between the Fe(III) mineral particles (i.e. Fig.1a area 2-3). From the Fe chemical maps, we conclude that Fe(II) is uniformly distributed in the background C-rich matrix and is not composed of particles that we can resolve with the microscope's spatial resolution of 30 nm. In fact, the Fe STXM image is consistent with adsorbed Fe as discussed above. How can we distinguish adsorbed or complexed Fe from uniformly distributed Fe-bearing particles <30 nm? We compare the experimental Fe NEXAFS spectra to those from reference materials to deduce its chemical form and find that the plume Fe(II) does not match any of the Fe-bearing minerals one would expect to find in the vicinity of MOR hydrothermal venting (e.g. Fig.S5). This tells us that the Fe(II) is not associated with Fe(II)-bearing minerals with diameters <30 nm. Because Fe L-edge NEXAFS spectra are diagnostic of a specific Fe form only in relationship to reference spectra, our interpretation is limited by the contents our reference spectral library and published spectra. Our reference library consists of many Fe-bearing minerals relevant to hydrothermal vent systems, so we have good confidence in our interpretation. It is our intention to build a Fe-organic database in response to our findings. If the Fe(II) we observe is not in the form of a nanoparticulate mineral, what form is it in?

At this stage, we turn our attention to the properties of the C-rich background matrix that is co-located with the Fe(II) in question. Our logical progression is this: the Fe(II) is uniformly distributed through out the C-rich background matrix, and it is not dissolved or in an Fe-bearing mineral, but has properties consistent with sorption-complexation. What is present in the C-rich background matrix that could sorb-complex Fe(II)? Carbon K-edge NEXAFS spectra are sensitive to electronic transitions in C-containing functional moieties. The C K-edge reference spectra demonstrate the sensitivity of the spectra to different classes of organic molecules (Fig.2 and Fig.S6). Spectra recorded on the C-rich background matrix show that it is composed of organic C with spectral features consistent with broad classes of biomolecules such as proteins, polysaccharides, and lipids. The composition of the matrix seems very much like a microbial biofilm with many different organic functional groups capable of sorbing-complexing cations, including Fe(II) and Fe(III). At this point in our data analysis, we interpret our results to be absolutely consistent with Fe(II) adsorption to functional groups or complexation by organic molecules present in the POC matrix.

Mineralogy and Iron Speciation in the ≥ 10 μm Diameter Fraction – At the micron scale, the Fe K-edge X-ray absorption near structure (XANES) spectroscopic measurements, in combination with X-ray diffraction (XRD) patterns, indicate that there are at least 8 different Fe species. In order to document sample complexity and heterogeneity, we have present examples of complementary data in Fig.S2-S4. With a beam spot size minimum of ~10 μm^2 we measure:

- ***X-ray fluorescence (XRF) maps and spectra*** for elemental composition (S, Ca, Ti, V, Mn, Fe, Ni, Cu, Zn, As, Se, Pb, and Sr monitored).

- ***Fe K-edge XANES spectra*** for Fe oxidation state, but mostly for relative proportion Fe-bearing mineral species. These data allow us to identify the major mineral group resent and in a few cases to identify the mineral itself, e.g. Fe sulfide minerals like pyrite or pyrrhotite. One does not model XANES data coordination environment because the energy range is too short. Our XANES data are compared to a large Fe XANES database (containing about 60 compounds[2]), fit by least squares method with linear combinations of references giving the relative proportions of Fe species, and subjected to PCA and target transformation analyses.

- ***XRD*** in transmission mode for mineral identification.

The EPR Tica vent hydrothermal particles were collected and treated as described in the Methods section, with the exception that the samples were analyzed directly after deposition onto polycarbonate (PC) membrane filters. The PC filters were analyzed at the ALS micro-probe beamline 10.3.2[3] under ambient conditions (air-dry, room temperature). Large areas (~ 1 mm^2) of the PC filter were mapped by micro X-ray fluorescence (μXRF) with 10 × 10 μm pixels, a 7 μm x 7μm incident beam, and using a seven-element Ge solid-state fluorescence detector. The XRF map of hydrothermal particles displayed in Fig.S2 is a composite map obtained from four XRF maps collected at: (1) 13 keV, (2) 100 eV above the Mn 1s-edge, (3) 50 eV above the V 1s-edge, and (4) 50 eV below the V 1s-edge. This multi-mapping strategy was used to distinguish between overlapping X-ray fluorescence lines: Mn K-α from Fe K-β, and V K-α from Ti K-β. Custom LabView programs available at the beamline were used to deadtime correct, register individual XRF maps, and combine specific fluorescence channels from individual maps into a single composite map. Discrete particles/aggregates with distinct chemical composition were then examined by recording XRF spectra at an incident energy of 17 keV. Micro-XRD patterns were recorded in transmission mode with a CCD camera (Bruker SMART6000, SMART software) at an incident energy of 17 keV (λ = 0.729 Å) and with exposure times of 240 s. XRF spectra and XRD patterns were also collected "off" of the particles of interest for background subtraction purposes. Two dimensional μXRD patterns were radially integrated to obtain one dimensional XRD profiles in Q space:

$$Q\ (\mathrm{nm}^{-1}) = 20\ \pi\ /\ d\text{-}spacing\ (\text{Å}).$$

DOI: 10.1038/NGEO433

Calibration of the energy and CCD-sample distance were performed using an Al_2O_3 standard and all XRD data were processed using the freeware program Fit2D[4]. The background substracted XRD patterns are presented in Fig.S3. Fe 1s-edge XAS spectra were also collected for further mineral identification (Fig.S3 and Fig.S4). The spectra were deadtime corrected, pre-edge background subtracted, and normalized in the post edge region. Linear least-squares (LSQ) fitting of XAS spectra was performed using a library of over 60 Fe reference spectra (Fig.S4)[2]. The best LSQ fit was obtained for minimum normalized sum-squares residuals:

$$NSS = 100 \times \{\sum(\mu_{exp} - \mu_{fit})^2 / \sum (\mu_{exp})^2\}$$

in the 7010-7410 eV range, where μ represents the normalized absorbance. In the case of spectra collected from Fe enriched particles, we corrected the spectra for over-absorption induced distortion in the following manner:

$$\mu_{corrected} = \mu_{exp} / (1 + a\,(1 - \mu_{exp}))$$

where the parameter a was adjusted to obtain the best match between the corrected spectrum and the combination of standard spectra. This simple model assumes the sample to be infinitely thick. The error on the percentages of species present is estimated to ± 10%. All XAS data processing was performed using a suite of LabView programs available at the beamline.

Our results show that a suite of complementary, spatially resolved techniques are required to understand Fe mineralogy and reactivity in hydrothermal plume particles. Specifically, we used XRF mapping to determine the elemental distributions among particles, XRD to query the X-ray diffracting minerals present, and Fe XAS to measure the proportion of specific Fe bearing phases as well as probing non X-ray diffracting minerals. The XRF maps demonstrate that Fe is an ubiquitous component of hydrothermal particles (Fig.S2). Iron was often associated with numerous other elements such as S, Ca, Zn, Cu, As and Se, indicating that the speciation and mineralogy of Fe is heterogeneous in these materials. The Fe bearing particles fell into four basic categories: (1) Fe sulfide minerals, predominantly pyrite, (2) weathered pyrite, i.e. Fe oxyhydroxide *plus* pyrite, (3) basalt derived minerals and glass, and (4) biological debris.

The sulfide minerals identified by XRD include pyrite (FeS_2), marcasite (FeS_2), sphalerite (ZnS), and chalcopyrite ($CuFeS_2$). Although many sulfide minerals are present, Fe XANES fitting results indicate that pyrite is indeed the major form of Fe within the particles of these sizes (≥ 10 μm). However, the LSQ fit was significantly improved by the addition of a pyrrhotite for one case (Fig.S4). As the XRD patterns do not exhibit any pyrrhotite peaks, Fe XANES results suggest the presence of poorly crystalline Fe sulfide minerals in the particle aggregates. Complementary data for these particles reveal that the dominant sulfide mineral pyrite is very closely associated with other sulfide minerals and has variable trace element composition. For example, both As-rich and Se-rich sulfide mineral particles were identified (As and Se not co-located), where some particles are enriched in Cu and Se (spot 7) and others enriched in As and Zn (spot 6). We also observed pyrite in close association with oxidized Fe minerals. While the XRD analysis did not detect Fe oxyhydroxide minerals, Fe XANES fitting results

indicate that the Fe-bearing materials within the particle are predominately pyrite (61 %) and 2-line ferrihydrite (39 %).

Basalt fragments, both glass and olivine, were also detected in the plume particles via Fe XANES analysis. The basaltic materials were enriched in Ca, Ti, V, Mn, and Fe. As with biological detritus (spot 5 and 8), the basalt derived materials are not considered authentic plume particulate material, i.e. they are entrained from near-vent deep-sea water or resuspended by deep ocean currents. However, these Fe-rich materials represent important components, numerically and chemically, of the near-vent suspended and descending particulate load.

DOI: 10.1038/NGEO433

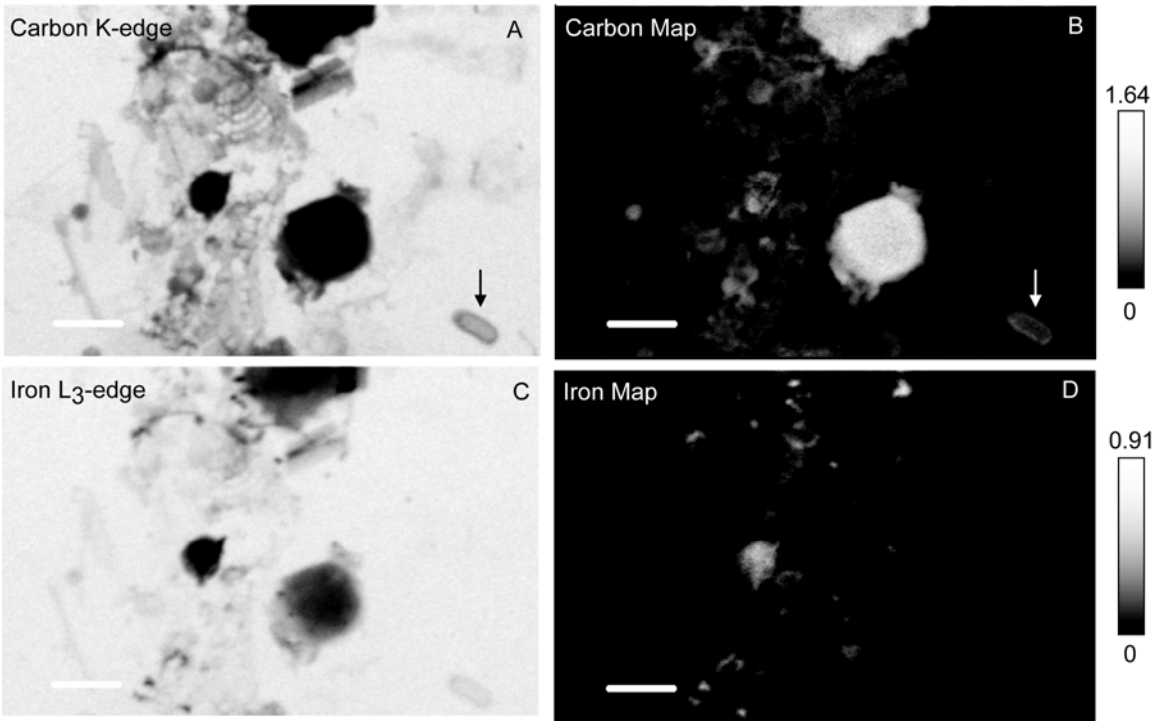

Fig.S1. Distribution of C and Fe on aggregates and biological detritus collected from the Tica vent sediment trap. Arrows in panels (A) and (B) point to the microbial cell whose C 1s spectrum is shown in Fig.2 and Fig.S6. (A) STXM image collected at C 1s edge (300 eV). (B) Carbon distribution map displayed in optical density units. (C) STXM image collected at Fe $2p_{3/2}$ edge (709.5 eV). (D) Fe distribution map, displayed in optical density units. Scale bars are 2 μm.

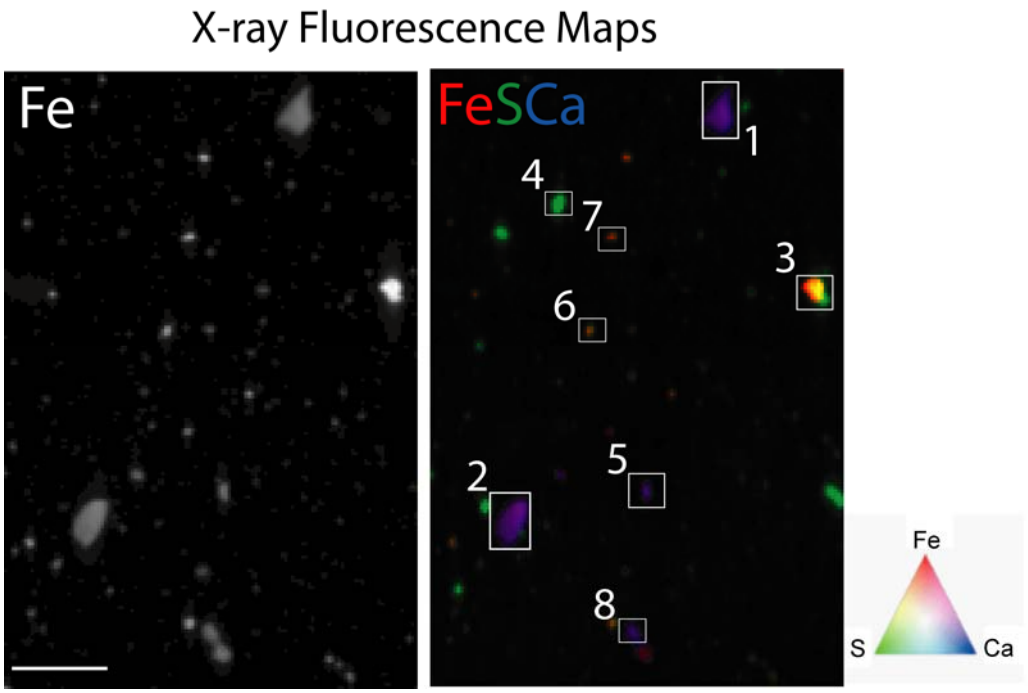

Fig.S2. X-ray fluorescence maps (Fe and tricolor-coded FeSCa) of Tica vent hydrothermal plume particles. Note, the same region of the filter is displayed in each of the four XRF maps, but different elemental distributions are chosen for display. Scale bar is 200 μm. The specific particles numbered 1 through 8 were further examined.

DOI: 10.1038/NGEO433

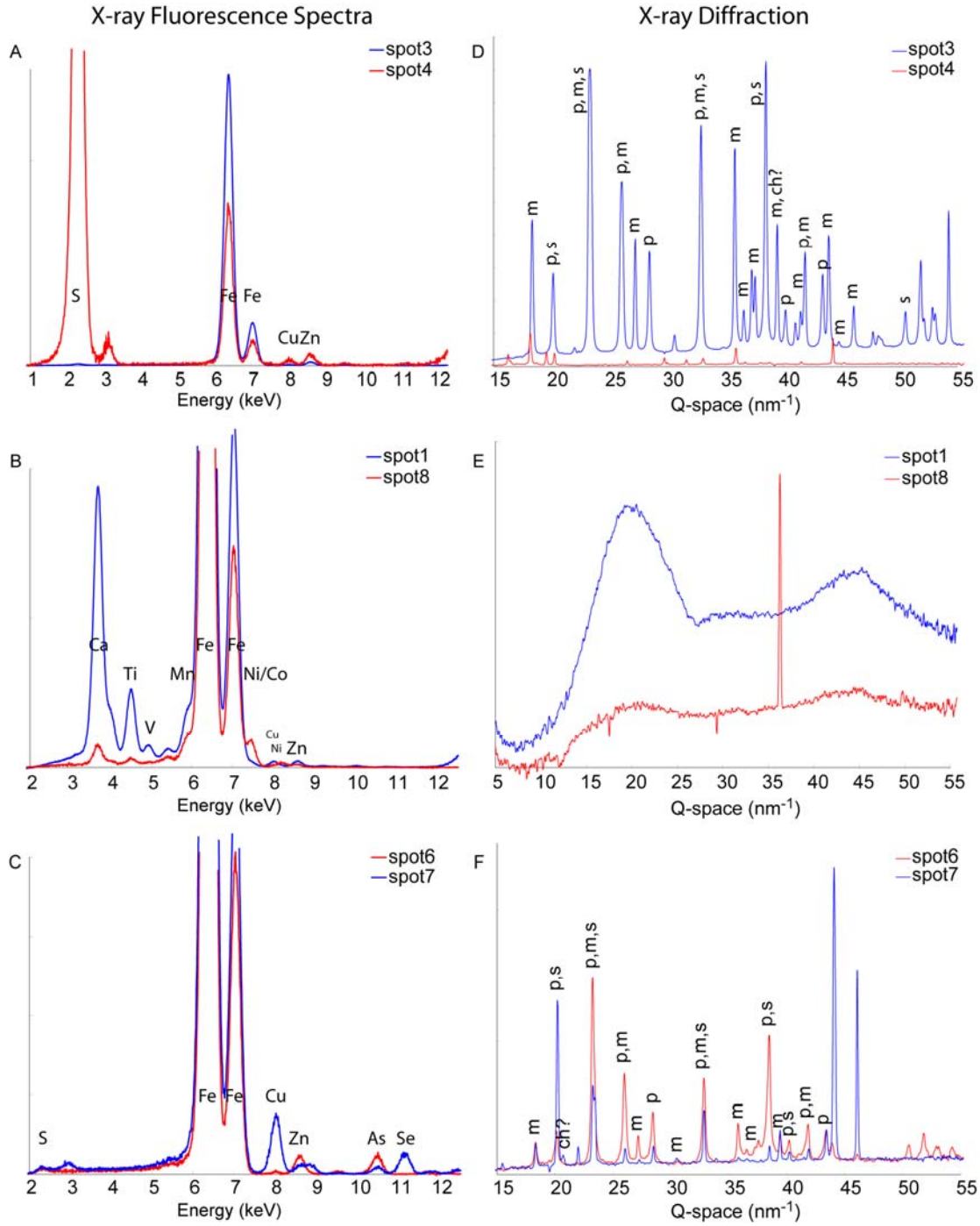

Fig.S3. X-ray fluorescence spectra (A-C) and X-ray diffraction patterns (D-F) for each particle/aggregate or "spot", spots 3 and 4 (A and D), spots 1 and 8 (B and E), and spots 6 and 7 (C and F) labeled on X-ray fluorescence maps displayed in Fig.S2. The y-axis range for the XRF spectra is constrained to allow viewing of the trace element peaks. X-ray diffraction peaks are labeled m (marcasite), p (pyrite), s (sphalerite), and ch (chalcopyrite).

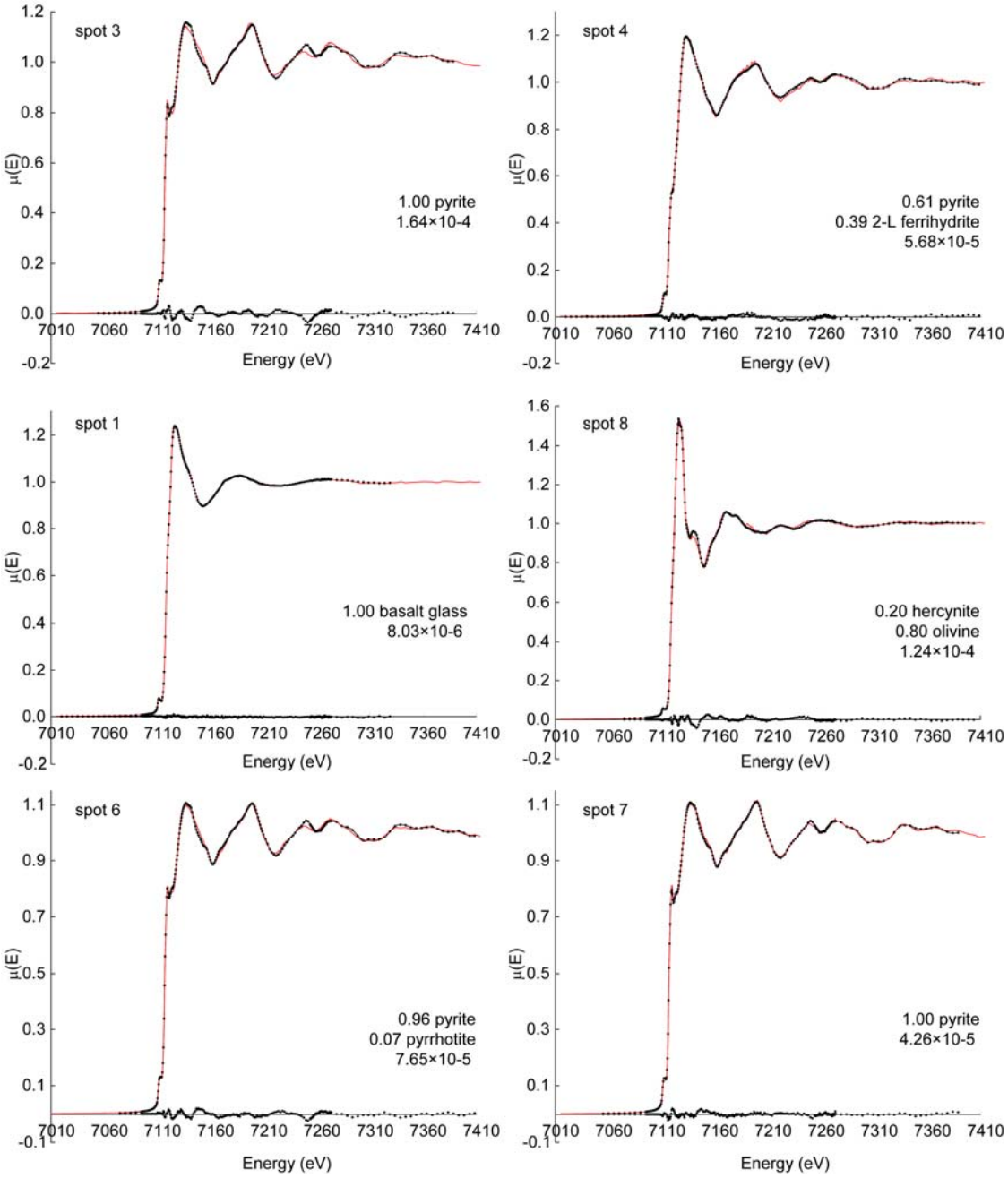

Fig.S4. Linear least-squares fitting results for normalized Fe 1s-edge XANES spectra collected from spots 1, 3, 4, 6, 7, and 8 (location of spots indicated on XRF maps in Fig.S2). Each panel in the figure is composed of the experimental data (red line), the best fit (dotted line), and fit residual or mismatch between the fit and the data (dotted line centered on the x-axis). The spectral components, fitted proportions, and goodness of fit parameter (normalized sum-squares residuals), are reported for each spot (e.g. the experimental spectrum from spot 4 was best fit as a combination of two reference spectra, 61 % pyrite and 39 % 2-line ferrihydrite.) The olivine reference material is $(Mg_{0.8}Fe_{0.2})SiO_4$ and the hercynite reference material is $FeAl_2O_4$.

DOI: 10.1038/NGEO433

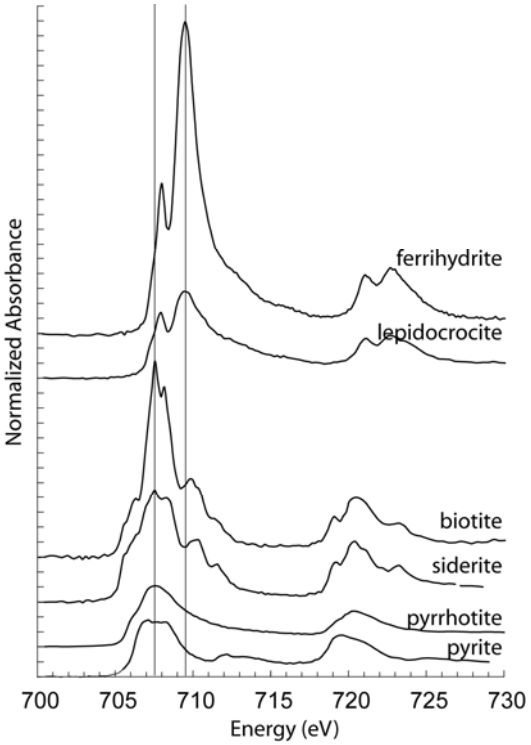

Fig.S5. Iron 2p spectra collected from Fe(II)- and Fe(III)-bearing reference minerals: ferrihydrite (Fe^{III} (oxyhydr)oxide), lepidocrocite ($Fe^{III}OOH$), biotite ($K(Mg,Fe^{II})_3AlSi_3O_{10}(OH,F)_2$), siderite ($Fe^{II}CO_3$), pyrite ($Fe^{II}S_2$), and pyrrhotite ($Fe_{1-x}S$, $0 \leq x \leq 0.2$). Vertical lines are displayed to show the characteristic Fe(II) and Fe(III) peak at 707.6 and 709.5 eV, respectively.

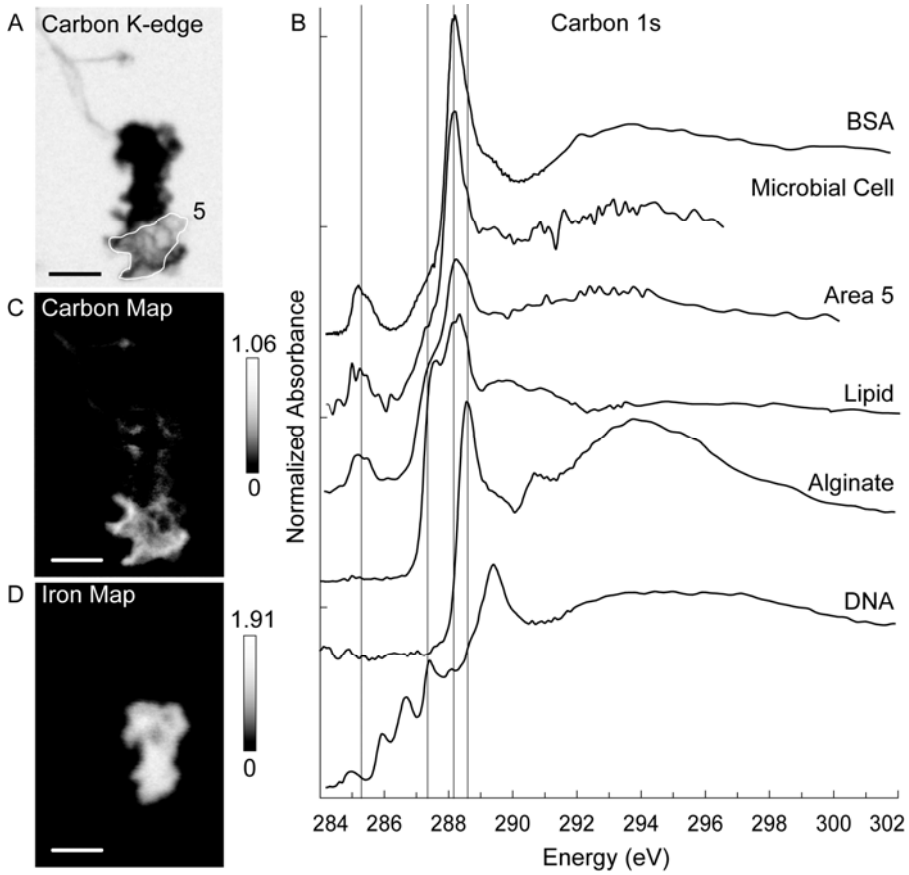

Fig.S6. Carbon spectromicroscopy of a particle aggregate collected from the Tica vent sediment trap (June 15-17, 2006). (A) STXM image collected at C 1s edge (300 eV) of particle aggregate. (B) Carbon 1s spectrum extracted from area 5 of the sample outlined in white in panel A, along with reference spectra from protein (BSA, bovine serum albumin), Tica vent microbial cell, lipid (1,2-dipalmitoyl-sn-glycero-3-phosphoethanolamine), polysacharride (alginate), and nucleic acid (DNA). Carbon and Fe distribution maps are displayed in panels (C) and (D), respectively. Scale bar is 1 μm. All elemental distribution maps are displayed in optical density units.

DOI: 10.1038/NGEO433

1. Toner, B. *et al.* Spatially resolved characterization of biogenic manganese oxide production within the biofilm of *Pseudomonas putida* strain MnB1. *Appl. Environ. Microbiol.* **71,** 1300-1310 (2005).
2. Marcus, M. A., Westphal, A. J., and Fakra, S. Classification of Fe-bearing species from K-edge XANES data using two-parameter correlation plots. *J Synchrotron Rad.* **15,** 463-468 (2008).
3. Marcus, M. A. *et al.* Beamline 10.3.2 at ALS: a hard X-ray microprobe for environmental and material sciences. *J. Synchrotron Rad.* **11,** 239-247 (2004).
4. Hammersley, A. P. *et al.* Two-dimensional detector software: From real detector to idealized image or two-theta scan. *High Press. Res.* **14,** 235-248 (1996).